



## Special Feature: Powertrain and Environment

Research Report

### Combustion Visualization Using Newly-developed Optically Accessible Single-cylinder Engines

Takayuki Fuyuto, Yoshiaki Hattori, Taketoshi Fujikawa and Kazuhiro Akihama

Report received on May 10, 2013

■**ABSTRACT**■ In-cylinder visualization using optically accessible engines has been an important tool for the detailed analysis of the in-cylinder phenomena of internal combustion engines. It is also essential for validating the accuracy of 3-dimensional numerical simulations. Most current optically accessible engines are recognized as being limited in terms of their speed and load, however, because of the fragility of certain components such as the transparent windows, as well as the inertia force arising from the heavy elongated piston. To overcome these speed and load restrictions, we developed a new generation of optically accessible engines which extend the operating range up to speeds of 6000 rpm for the spark-ignition (SI) engine version, and up to in-cylinder pressures of 20 MPa for the compression-ignition (CI) engine version. To compensate for the inertia force associated with the elongated piston, we used two opposing balancing pistons, in a perfectly balanced configuration.

This paper describes the features of the newly developed optically accessible engines and provides some examples of in-cylinder visualization. One example is a visualization of the flame propagation in SI combustion at 5000 rpm. Another is a CO laser induced fluorescence (CO-LIF) imaging in diesel combustion with multiple injections.

■**KEYWORDS**■ Combustion, SI Engine, Diesel Engine, Visualization, LIF, Measurement, Flame Propagation, CO

#### 1. Introduction

A precise understanding of in-cylinder phenomena, such as fuel injection, air-fuel mixing, combustion and emissions formation, is essential to improving the combustion process and reducing engine emissions and fuel consumption. To understand these in-cylinder phenomena, in-cylinder visualization with optical access has been an important tool.

Recently, there has been considerable improvement in the accuracy of numerical simulation for predicting in-cylinder pressure and the rate of heat release. However, the accuracy of simulation still falls short when attempting to predict NO<sub>x</sub>, soot, CO, and unburned hydrocarbon emissions. We thus rely on in-cylinder visualization for validating our simulation models, such as the spray break-up model and combustion model, as well as for adjusting the parameters of those models.

The techniques for visualizing in-cylinder phenomena can be categorized into two types. One is

the use of an end-scope which is inserted into one cylinder of an actual multi-cylinder engine. The set-up for this method is relatively easy, although it does present some disadvantages, such as a narrow field of view and the distortion of the captured images. The other method involves the use of an optically accessible single-cylinder engine with an elongated piston (**Fig. 1**). With the basic bottom-view arrangement, the in-cylinder phenomena can be observed through a combination of a window mounted at the top of the elongated piston and a mirror. The mirror is mounted on the cylinder block, angled at 45 degrees to the vertical. The set-up for this method involves considerable effort, not least in the manufacture of the engine and its elongated piston. The method does, however, offer several advantages, notably, a wide field of view and images that are not distorted.

The bottom-view configuration using an elongated piston was originally developed by Bowditch in 1961 and was used to visualize SI combustion.<sup>(1)</sup> Since then,

this configuration has been widely used not only for SI engines, but also for diesel engine analysis, while the field and direction of view have been extended.<sup>(2-13)</sup> In addition to the bottom-view window, some optically accessible engines have a transparent cylinder that can be accessed from the side to observe phenomena which vary in the vertical direction, or to irradiate the laser light used in laser diagnostic techniques.

Laser diagnostic techniques are powerful tools for visualizing phenomena that cannot be observed by direct photography methods.<sup>(8-13)</sup> The 2-D distributions of fuel vapor and NO<sub>x</sub>, for example, can be visualized using the planar laser-induced fluorescence (P-LIF) technique. A thin laser sheet is introduced into the combustion chamber as an excitation light source for LIF imaging. To observe a horizontal distribution, in general, a laser sheet is projected through the transparent window or cylinder that is mounted just below the cylinder head. LIF images can thus be captured through the transparent piston.

Most existing optically accessible single-cylinder engines are, however, recognized as being limited in terms of speed and load, because of the fragility of certain components such as the elongated pistons and transparent windows. They are limited to speeds of less than 3000 rpm. There have, nevertheless, been a few optical single-cylinder engines that can run at high

speeds and/or under high loads. The gasoline engine developed by Pitcher et al. can run at 5000 rpm without combustion.<sup>(7,8)</sup> The diesel-type engine developed by Hotta et al. lets us visualize combustion at high speeds of 4000 rpm and under high loads (maximum in-cylinder pressure = 12 MPa).<sup>(6)</sup> However, the operating ranges of actual gasoline and diesel engines cannot be duplicated by current optically accessible engines.

To overcome these speed and load restrictions, a new generation of optically accessible engines was developed which extends the operating range to 6000 rpm for the SI engine version, and to in-cylinder pressures of 20 MPa for the CI engine version.<sup>(14)</sup>

This paper describes the details and features of newly developed optically accessible engines and provides some examples of in-cylinder visualization. One example is a visualization of the flame propagation in SI combustion at 5000 rpm. Another is the CO-LIF imaging in diesel combustion with multiple injections.<sup>(15,16)</sup>

## 2. Development of SI Engine Version

### 2.1 Problems That Occur at High Speeds

The main reason for imposing a speed limit on an engine is the inertia force created by the heavy elongated piston, with its wide bottom-view window. This inertia force increases with the square of the engine speed. Increasing the speed to over 6000 rpm leads to the appearance of two new problems. The first is mechanical damage to the crankshaft. The inertia force acting on the elongated piston and connecting rod combine to apply a bending force to the crankshaft. The second is friction damage to the shaft bearings. The crankshaft is consistently pushed in the direction of the connecting rod, thus inducing friction damage in the shaft bearings.

To overcome these two problems, it is necessary to increase the mass of the counterweight and so establish an "overbalance." The authors increased the mass-moment of the counterweight to minimize the bending force and the bearing surface pressure. This increase in the counterweight mass-moment, however, results in an imbalance.

The top-left part of **Fig. 2** illustrates a balancing mechanism that is commonly used in existing optically accessible single-cylinder engines. Many optical engines have balancer shafts that rotate symmetrically to compensate for the vertical inertia force of the

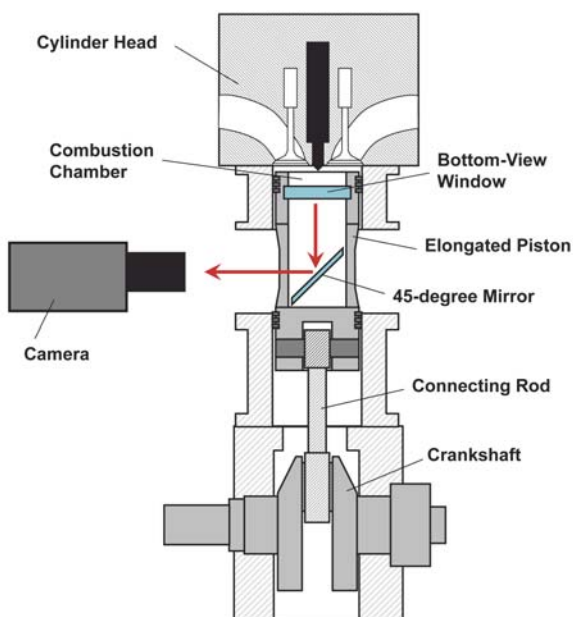


**Fig. 1** The bottom-view type optically accessible single-cylinder engine with an elongated piston.

elongated piston and the smaller end of the connecting rod. Some optical engines only have 1st-order balancers. Others, which are designed to operate at high speed, have 2nd-order balancers rotating at twice the speed of the crankshaft which cancel out the 2nd-order inertia force on the elongated piston. The horizontal inertia force induced by the centrifugal force on the larger end of the connecting rod and the crankshaft is canceled by the counterweight attached to the crankshaft, while the overbalance rate is designed to be 0%. The bottom-left part of Fig. 2 shows the results of FEM analysis on a crankshaft with an overbalance rate of 0%, assuming that it rotates at a high speed of 8000 rpm, thus introducing a considerable margin. The inertia force and centrifugal force acting on the elongated piston and connecting rod combine to apply a bending force to the crankshaft. The maximum value of the local stress induced by the bending force exceeds the limit. On the other hand, this maximum value can be reduced if the counterweight mass-moment is increased to establish an overbalance condition (Fig. 2, bottom-right). Each increment in the

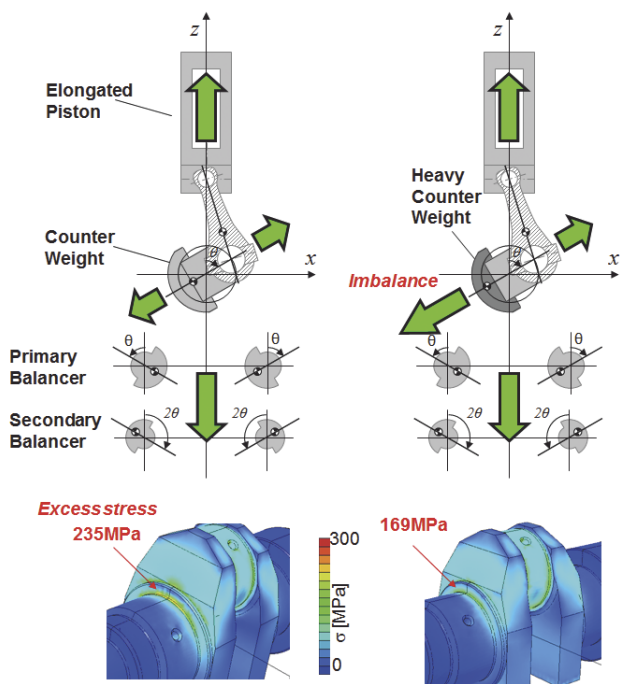


**Fig. 2** (top-left) The basic balancing mechanism of optically accessible engines with an elongated piston and (top-right) an imbalance induced by overbalance condition with a heavy counter weight. (bottom) Stress distribution calculated by FEM (@TDC, 8000 rpm).

centrifugal force, however, induces an imbalance (Fig. 2, top-right).

## 2.2 Perfect Balance System

The authors set out to devise a new balance system. A comparison of the boxer type, straight type, etc. shows that the boxer-twin is the ideal arrangement of pistons, since the main cylinder and the opposed “sub” cylinder attain a point-symmetry with respect to the crank axis in the  $xz$ -2D plane and thus compensate for each other’s inertia force (Fig. 3). This simple boxer-twin, however, induces a moment in the  $yz$ -2D plane since the sub-cylinder is not on the same straight line as the main cylinder but is instead shifted back in the  $y$ -direction.

Therefore, the authors devised the vertically opposed perfect balance system shown in Fig. 4. The two

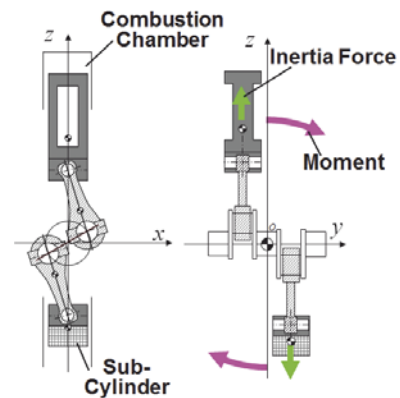


**Fig. 3** Imbalance of the boxer-twin type engine.

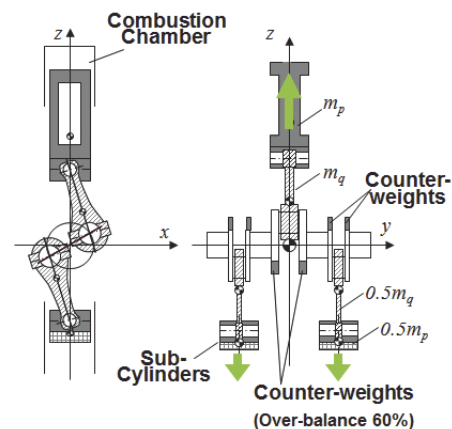


**Fig. 4** Vertically opposed perfect balance system.

opposing sub-cylinders are arranged in front of and behind the main cylinder, with a weight ratio of “1:2:1.” The resultant of the inertia forces of the two sub cylinders perfectly compensates for that of the main cylinder without the emergence of the moment in the  $yz$ -2D plane. In addition, heavy counterweights with an overbalance rate of over 60% are attached to both the main and sub cylinders to prevent either mechanical damage to the crankshaft, or friction damage to the shaft bearings. Trial operation of a prototype SI engine version with “metal windows” instead of transparent glass windows revealed that a maximum speed of 6000 rpm could be achieved. Subsequently, we successfully performed in-cylinder visualization with transparent windows at 5000 rpm.

### 2.3 SI Engine Version of Optically Accessible Single-cylinder Engine

**Figure 5** shows a schematic of the combustion chamber of the SI engine version. Full optical access to the pent-roof area from the engine side is possible, because the top of the transparent cylinder is formed into a highly precise pent-roof shape. This engine has a bore and stroke of 86 mm × 86 mm. A special ceramic coating is applied to the inner surface of the cylinder liner and the upper skirt surface of the elongated piston and piston ring surface so as to realize high-speed and long-term operation with no lubricating oil, allowing the window to remain clean during imaging.

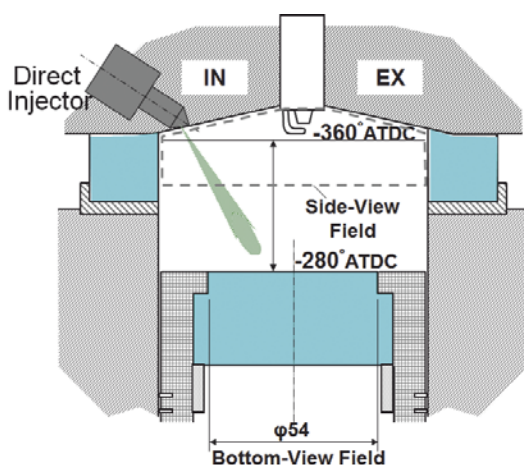


**Fig. 5** Schematic of the combustion chamber of the SI engine version.

## 3. Development of CI Engine Version

### 3.1 Elongated Piston with New Structure

We have also developed a CI version, based on the SI version. The bore is 86 mm, the same as the SI version, but the stroke is extended to 96 mm. The development targets for the CI version were a maximum speed of 5000 rpm and a maximum in-cylinder pressure of 20 MPa. The speed target of 5000 rpm was achieved by adopting the same perfect balance system as that used for the SI version.

Key to the CI version development was the new structure of the elongated piston. The left part of **Fig. 6** shows the results of a FEM analysis of the stress distribution in a conventional elongated piston, assuming the maximum in-cylinder pressure to be 20 MPa. In this case, the opening in the elongated piston bulged out to the left and right as a result of the heavy load on the top of the piston. Thus, stress concentrations appeared at the upper corners of the opening and reduced the safety factor to 1.56, indicating that the piston is not strong enough. For cyclic loading, we should have a safety factor of at least 3.0. Therefore, the authors made major improvements to the shape of the elongated piston and the 45-degree mirror, shown in Fig. 6 (right). First, the shape of the 45-degree mirror was minimized, such that only the center part of the mirror was ultimately left. Secondly, the length of the opening was shortened by eliminating the visualization facility around BDC,

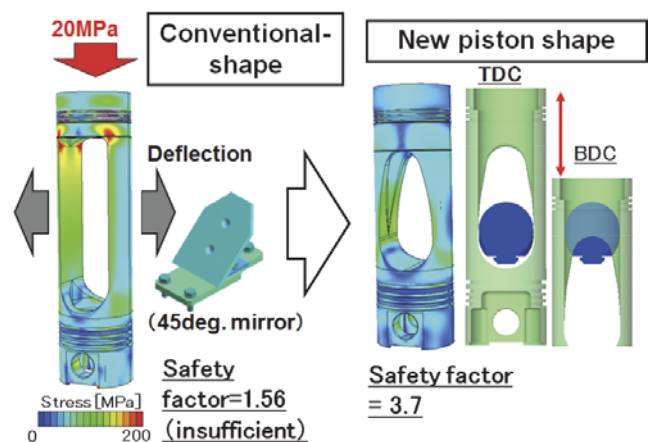


**Fig. 6** Improvements of elongated piston and 45 degree mirror.

since in-cylinder visualization is required around TDC only for diesel combustion analysis. We were thus able to reduce the total length of the elongated piston. Furthermore, an egg-shaped opening was devised and adopted to disperse the stress concentrations at the upper corners of the opening. As a result, the safety factor under an in-cylinder pressure of 20 MPa was increased to 3.7.

### 3.2 Improved Optial Access

In the case of a diesel engine with a common-rail injection system, fuel is injected into the squish area as well as into the piston cavity in the early pilot or after the injection stages. To clearly observe the in-cylinder phenomena from the piston cavity to the squish area, the authors previously developed an optically accessible single-cylinder engine that let us observe the combustion chamber from three directions; from the bottom, from the top, and from the side.<sup>(13)</sup> The new CI version also features this design, allowing optical access from three directions (Fig. 7). The material used for the bottom and top windows is synthetic sapphire, instead of the synthetic quartz used conventionally, to resist the high in-cylinder pressure.

The piston cavity of an actual DI diesel engine has a conical rather than a flat bottom surface. If in-cylinder visualization is required using the same combustion chamber, so as to reproduce the flow pattern of the actual engine, the authors use bottom-view windows having the shape shown in Fig. 8 (b). If the upper surface were to be conical and the bottom surface flat

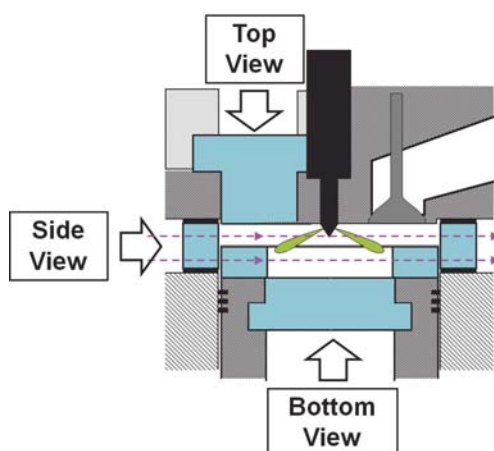


Fig. 7 Schematic of the combustion chamber of CI engine version.

(Fig. 8 (a)), the observed image would be blurred. Therefore, the lower surface of the window is conical so as to parallel the upper surface, such that light rays remain parallel as they pass through the bottom window. This enables us to apply shadow-graph visualization from the bottom, and eliminates the blurring of images. A problem remains, however, in that the parallel light rays shift inwards when they pass down through the bottom window. Image-processing is used to correct this inward shift. The result of applying the image-processing to a captured image of full-load diesel combustion is shown in Fig. 9.

### 4. Visualization of High Speed Direct-injection Spark-ignition (DISI) Combustion

A visualization of the flame propagation in DISI combustion at 5000 rpm was performed by using the SI engine version. There are other methods of measuring flame propagation in SI combustion under high-speed conditions other than direct visualization

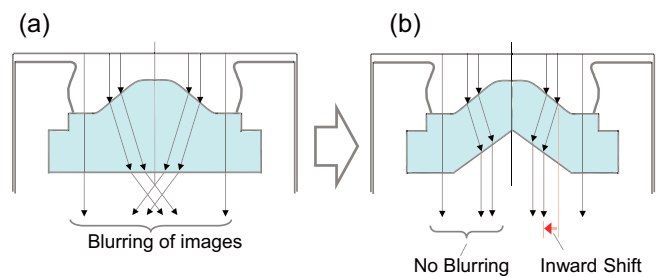


Fig. 8 A bottom view sapphire window having a pair of conical shape surfaces.

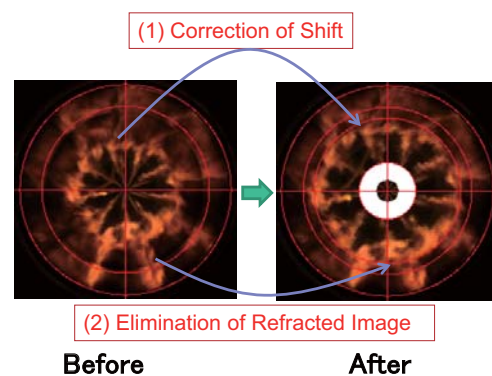


Fig. 9 Result of applying the image-processing to a captured image of full load diesel combustion taken through the bottom-view conical sapphire window.

by a high-speed video camera, such as the ion-current probe method<sup>(17)</sup> and tomography.<sup>(18)</sup> The former method measures flame propagation by gathering the ion currents detected by multiple probes which are embedded into the surface of the cylinder head. The latter method detects chemical luminescence on multichannel optical paths by using a number of microfiber sensors implanted into the spark plug or the cylinder-head gasket. These methods, however, have a lower spatial resolution and incur complicated data processing. There is a need, therefore, for a method of direct visualization using an optically accessible engine and a high-speed camera.

Flame propagation was directly observed by a high-speed video camera (Photron FASTCAM SA1.1) from both the piston side and bottom at an engine speed of 5000 rpm. The frame speed was 20,000 fps. The engine load was 200 kPa at IMEP and the fuel-air mixture was stoichiometric. The fuel was directly injected into the cylinder during the intake stroke by a DI injector mounted under the intake port. The timings

of the intake valve movement, fuel injection, and ignition are shown in Fig. 10.

Typical observed side and bottom-view images are shown in Fig. 11. The results obtained at low engine speeds (1000 rpm) are also presented for comparison. At 1000 rpm, the flame propagation is almost uniform in the intake and exhaust valve directions. In contrast, the flame propagation is not uniform when the engine is running at 5000 rpm. The difference in the uniformity of the flame propagation can be clearly seen in the bottom-view photographs, shown in Fig. 12. The shapes of the flames are almost concentric when the engine is operating at 1000 rpm. At 5000 rpm, however, the flame propagates more quickly towards the exhaust valve side. It is thought that this asymmetric flame propagation can be attributed mainly to the remnant tumble flow up until TDC, from the spark plug to the exhaust valves near the cylinder head surface. There is also the possibility, however, that the non-homogeneity of the air turbulence and the air/fuel mixture leads to asymmetric flame

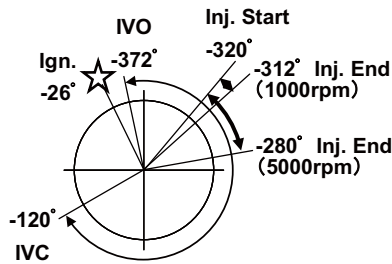


Fig. 10 The timings of intake valve movement, fuel injection and ignition.

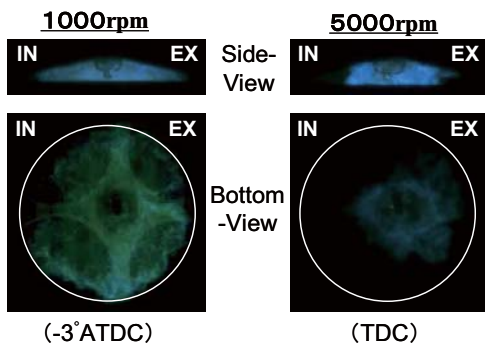


Fig. 11 Typical observed side and bottom-view images of high-speed DISI combustion.

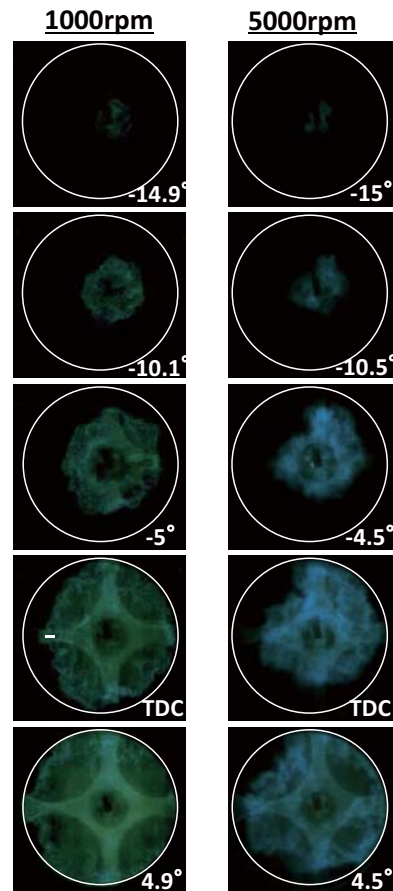


Fig. 12 The difference in the uniformity of flame propagation (bottom view).

propagation.

The authors will investigate the factors causing the asymmetric flame propagation by using the newly developed optically accessible engine, given that it has an operating range of up to 6000 rpm.

## 5. In-cylinder CO-LIF Imaging in Diesel Combustion

### 5.1 Background: Need for CO-LIF Imaging

A recent trend in diesel engine development is an increase in the EGR rate with the goal of lowering the combustion temperature to reduce NO<sub>x</sub> emissions, although this leads to an increase in carbon monoxide (CO) emissions. There is thus a need to reduce CO emissions by improving in-cylinder combustion when the temperature of the diesel oxidation catalyst (DOC) is lower than its activating temperature. To clarify the CO emission sources in diesel combustion, there is a need to detect the timing and location at which the reaction in the diesel combustion chamber where CO oxidizes to CO<sub>2</sub> stops. The methods available for identifying this timing and location are laser-induced fluorescence (LIF) imaging and 3-D numerical simulation. As mentioned in the introduction, however, the accuracy of numerical simulation still falls short when attempting to predict CO emissions. For example, Ekoto et al. compared in-cylinder LIF measurements with numerical simulations of low-temperature combustion.<sup>(19)</sup> The measured distributions of CO by LIF did not agree with the numerical simulations in terms of their location in the combustion chamber. Thus, numerical simulation is currently not a satisfactory analysis tool.

Therefore, an in-cylinder CO imaging technique based on two-photon excitation LIF for sooting combustion was developed. The accuracy of the numerical simulation was verified by comparing the results with the values obtained by CO-LIF imaging. Then, the major sources of CO emissions under low- and high-load conditions were analyzed using CO-LIF imaging and CFD simulation.

### 5.2 CO-LIF Imaging Technique and Numerical Simulation

Two-photon excitation CO-LIF imaging<sup>(20)</sup> was applied to the diesel combustion field with a luminous flame. CO molecules are excited from the ground state

( $X^1\Sigma^+$ ) to the excited state ( $B^1\Sigma^+$ ) by means of two-photon excitation at a wavelength of 230.1 nm. Fluorescence from the excited state to the lower-lying level ( $A^1\Pi$ ) at around 483 nm was detected. **Figure 13** shows the optical set-up for two-photon excitation CO-LIF imaging. An excitation laser beam was introduced into the combustion chamber through a non-luminescent quartz cylinder and then the CO fluorescence distribution was measured using an image-intensified CCD camera through the bottom-view sapphire window. The biggest hurdle faced in applying two-photon excitation CO-LIF imaging was the overlap of the blue color component of the luminous flame over the weak CO fluorescence. This was solved by optimizing the viewing direction and applying the off-line subtraction method.

Numerical simulations were performed by using AVL-FIRE, which supports the use of a series calculation methodology that links the three-dimensional two-phase nozzle internal flow calculation with the in-cylinder spray calculation, in order to improve the accuracy of the spray penetration and the mixture formation in the cylinder.<sup>(21)</sup> The ECFM-3Z combustion model was used to calculate the kinetic oxidation of CO.<sup>(22)</sup>

Further details of the CO-LIF imaging and the numerical simulation were reported in our previous papers.<sup>(15,16)</sup>

### 5.3 Validation of Numerical Simulation

A comparison of the CO distribution as obtained by

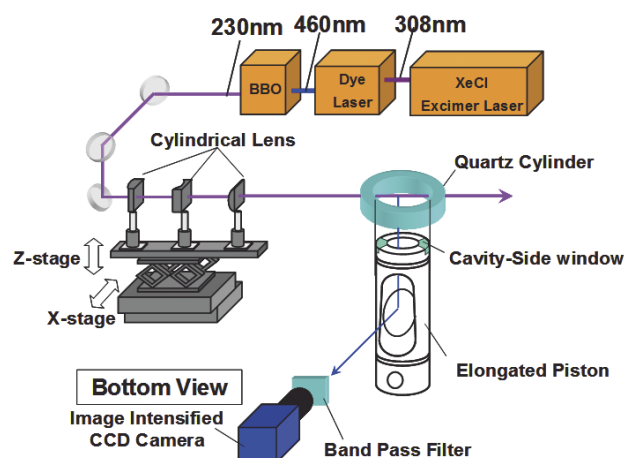


**Fig. 13** Optical set-up for two-photon excitation CO-LIF imaging using an optically accessible engine.

CO-LIF imaging and numerical simulation was done under low-load conditions in which a large amount of CO is emitted (Fig. 14). The injection pattern includes two pilot injections and a main injection. We measured a vertical cross-section through the cylinder axis and a horizontal cross-section 10 mm below the cylinder head. This vertical cross-section is located 15° downstream in the swirl direction relative to the spray angle. The imaging timing was 40° ATDC. The results of the simulation show that there is a dense, ring-shaped CO gas cloud above the piston cavity. The results of CO-LIF imaging through the vertical and the horizontal cross sections show part of this dense, ring-shaped CO gas cloud, which is indicated by the dotted line in the vertical cross-section. This comparison of the CO distribution results shows good agreement as to the location of the dense CO gas clouds.

To further validate the accuracy of the simulation, another comparison was performed (Fig. 15). The main injection was removed from the injection pattern under the low-load condition, leaving only two pilot injections. The imaging timing was advanced to 30° ATDC. Two cavity side-wall windows were fitted to the top of the elongated piston. The excitation laser-beam was used to sweep from the inside of the piston cavity to the vicinity of the cylinder head to observe a vertical

cross-section. Regarding the shape and location of the dense CO gas cloud emitted from the pilot flame (upper-left side of the dotted line), the CO-LIF image is in good agreement with the simulation.

As a result of these comparisons, we confirmed the reliability of the numerical simulation.

#### 5.4 Analysis of CO Emission Source

The CO emission source under low-load conditions was analyzed by using CO-LIF imaging, numerical simulation, and direct photography. The simulation and the CO-LIF imaging under the conditions without the main injection show that a large amount of CO was emitted from the pilot flame. The simulation results show that the pilot sprays diffuse excessively and form an over-lean mixture, preventing the local temperature from reaching the 1500 K that is required for CO oxidation. Therefore, the oxidation of CO stops, leaving large amounts of CO in the emissions.

Under low-load conditions with the main injection, part of the CO produced by the pilot flames is oxidized by the hot main flame. Figure 16 shows the results of simulation from TDC to 40° ATDC with direct photography of the main flame. The 3-dimensional figure shows an iso-surface of a CO mass fraction of 5% at 25° ATDC. In the inner region where the main flame is found, the local temperature rises to over 1500 K and the CO oxidizes completely. Under low-load

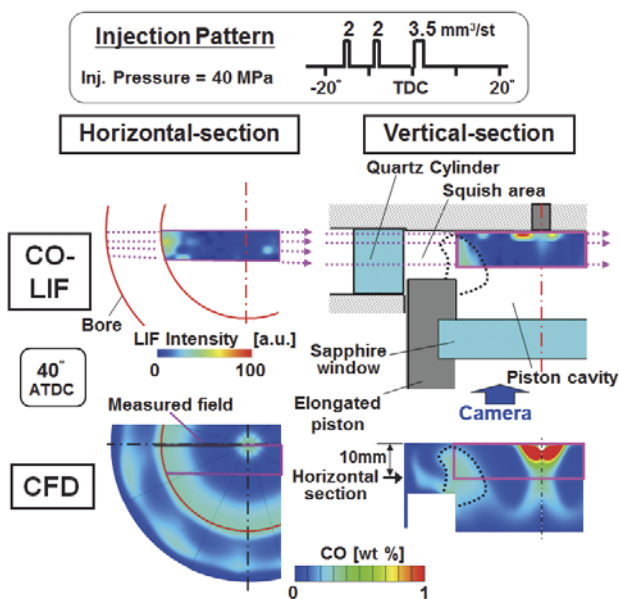


Fig. 14 Comparison of CO distribution between results of CO-LIF imaging and results of simulation under low-load conditions.

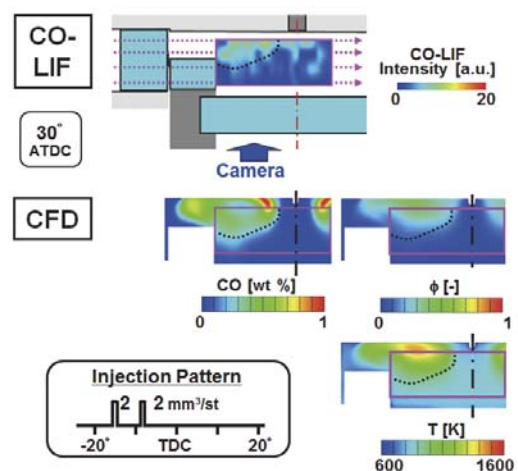


Fig. 15 Comparison of CO distribution between results of CO-LIF imaging and results of simulation under the condition without main injection.

conditions, however, the amount of fuel in the main injection is so small that gaps arise between the adjacent main flames, as shown by the direct photography. As a result, the CO gas clouds emitted from the pilot flames and existing in the gaps between the high-temperature main flames cannot be oxidized. In this study, we used CO-LIF imaging to visualize this CO gas cloud which was not oxidized by the main flames.

## 6. Conclusion

We have developed a new generation of optically accessible single-cylinder engines. The new design extends the operating range of optically accessible engines to high-speed and high-load conditions, which makes in-cylinder imaging analysis possible over the entire operating range of the actual engines.

The main issue occurring at high speeds was the vibration caused by the effect of the inertia force on the heavily weighted elongated piston. To compensate for the fact that the inertia force on the elongated piston increases with the square of the engine speed, a vertically opposed perfect balance system was devised.

This system has two opposing sub-cylinders arranged in front of and behind the main cylinder with a weight ratio of “1:2:1.” This extends the operating range of the SI engine version up to speeds of 6000 rpm.

The development target of the CI engine version was to extend the operating range to high loads, and specifically a maximum in-cylinder pressure of 20 MPa. The designs of the elongated piston and the 45 degree mirror were improved and an egg-shaped opening was devised to alleviate the stress concentrations.

Using the SI version, flame observations of DISI combustion, as observed from the side and from below, were performed at an engine speed of 5000 rpm. The uniformity of the flame propagation was clearly visible in the bottom-view photographs.

We measured the in-cylinder CO distribution in a diesel engine by means of two-photon excitation LIF using the CI engine version, in order to analyze the CO emission sources in diesel combustion with multiple injections. Then, the accuracy of the numerical simulation was verified by comparing the simulation results with the values obtained by CO-LIF imaging. We analyzed the CO emission sources in diesel combustion by using both in-cylinder CO imaging and numerical simulation.

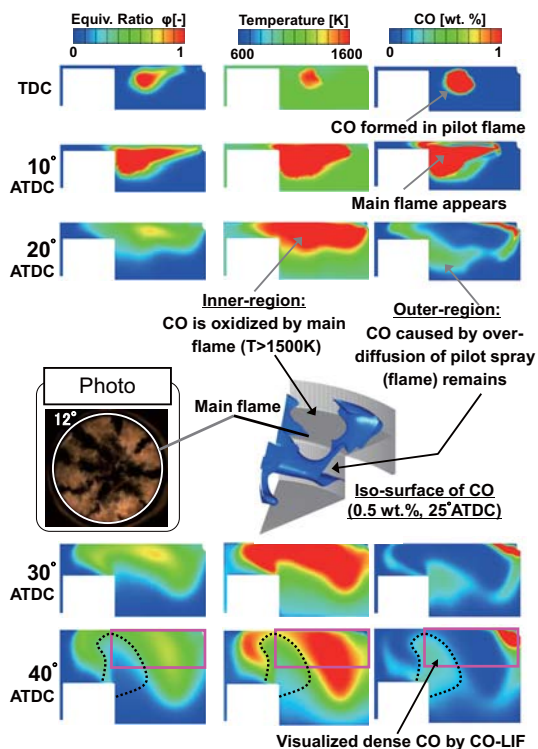


**Fig. 16** Detailed analysis of CO emission source under low-load conditions.

## Acknowledgments

The development of the new optically accessible engines was supported by Mr. Takafumi Matsumoto, Mr. Yuji Umemura, and Mr. Yoshitaka Mizuno of Toyota Central R&D Labs. The image-processing and the numerical simulation were supported by Mr. Ko Kugimoto and Ms. Reiko Ueda. The authors would like to acknowledge the support of Mr. Hisaki Ito and Mr. Akio Kawaguchi of Toyota Motor Corp., as well as Mr. Hideki Aoki and Mr. Tsutomu Umehara of Toyota Industries Corp. in our research into CO emission sources in diesel combustion.

## References

- (1) Bowditch, F. W., “A New Tool for Combustion Research: A Quartz Piston Engine”, *SAE Tech. Paper Ser.*, No. 610002 (1961).
- (2) Kozuka, K., et al., “Television System for Viewing Engine Combustion Processes and the Image Analysis”, *SAE Tech. Paper Ser.*, No. 810753 (1981).
- (3) Bates, S. C., “A Transparent Engine for Flow and Combustion Visualization Studies”, *SAE Tech. Paper*

- Ser., No. 880520 (1988).
- (4) Fujikawa, T., et al., "Development of Transparent Cylinder Engines for Schlieren Observation", *SAE Tech. Paper Ser.*, No. 881632 (1988).
  - (5) Mueller, C. J. and Martin, G. C., "Effects of Oxygenated Compounds on Combustion and Soot Evolution in a DI Diesel Engine: Broadband Natural Luminosity Imaging", *SAE Tech. Paper Ser.*, No. 2002-01-1631 (2002).
  - (6) Hotta, Y., et al., "Cause of Exhaust Smoke and Its Reduction Methods in an HSDI Diesel Engine Under High-speed and High-load Conditions", *SAE Tech. Paper Ser.*, No. 2002-01-1160 (2002).
  - (7) Allen, J., et al., "An Advanced Optically Accessed Single Cylinder Research and Development Engine for Fuel/Air Mixing and Combustion Diagnostics", *Proc. of 15th International Combustion Engine Symposium* (1999), pp. 595-600.
  - (8) Pitcher, G., et al., "The Effect of Early Valve Closing on Combustion within a Direct Injection Spark Ignition Engine", *Proc. of COMODIA* (2008), pp. 205-212.
  - (9) Arnold, A., et al., "DI Diesel Engine Combustion Visualized by Combined Laser Techniques", *Proc. of 24th Symposium (International) on Combustion* (1992), pp. 1605-1612.
  - (10) Fujikawa, T., et al., "Quantitative 2-D Fuel Distribution Measurements in an SI Engine Using Laser-induced Fluorescence with Suitable Combination of Fluorescence Tracer and Excitation Wavelength", *SAE Tech. Paper Ser.*, No. 972944 (1997).
  - (11) Akihama, K., et al., "Laser-induced Fluorescence Imaging of NO in a Port-fuel-injected, Stratified-charge SI Engine-correlations between NO Formation Region and Stratified Fuel Distribution", *SAE Tech. Paper Ser.*, No. 981430 (1998).
  - (12) Fujikawa, T., et al., "2-D Temperature Measurements of Unburned Gas Mixture in an Engine by Two-line Excitation LIF Technique", *SAE Tech. Paper Ser.*, No. 2006-01-3336 (2006).
  - (13) Fuyuto, T., et al., "Diesel In-cylinder Measurement Technique Using a Multi-direction Optically Accessible Engine", *Journal of Environment and Engineering*, Vol. 5, No. 1 (2010), pp. 72-83.
  - (14) Fuyuto, T., et al., "A New Generation of Optically Accessible Single-cylinder Engines for High-speed and High-load Combustion Analysis", *JSAE Paper*, No. 20119137 (*SAE Tech. Paper Ser.*, No. 2011-01-2050) (2011).
  - (15) Fuyuto, T., et al., "Analysis of CO Emission Sources in Diesel Combustion with Multiple Injections", *Proc. of COMODIA* (2012), pp. 287-292.
  - (16) Fuyuto, T., et al., "CO Emission Sources in Diesel Combustion with Multiple Injections and Reduction Techniques", *Proc. of THIESEL* (2012), 12p.
  - (17) Suzuki, Y., et al., "S. I. Engine Combustion Flame Propagation Measurement and Knocking Analysis by Ion Current Probes Including Moving Intake and Exhaust Valve Faces", *SAE Tech. Paper Ser.*, No. 2007-01-1420 (2007).
  - (18) Philipp, H., et al., "Localization of Knock Events in Direct Injection Gasoline Engines", *SAE Tech. Paper Ser.*, No. 2001-01-1199 (2001).
  - (19) Ekoto, I., et al., "UHC and CO Emissions Sources from a Light-duty Diesel Engine Undergoing Dilution-controlled Low-temperature Combustion", *SAE Tech. Paper Ser.*, No. 2009-24-0043 (2009).
  - (20) Seitzman, J., et al., "Quantitative Two-photon LIF Imaging of Carbon Monoxide in Combustion Gases", *Applied Optics*, Vol. 26, No. 14 (1987), pp. 2892-2899.
  - (21) Nagaoka, M., et al., "Modeling of Diesel Spray Atomization Linked with Internal Nozzle Flow", *R&D Review of Toyota CRDL*, Vol. 42, No.2 (2011), pp. 73-84.
  - (22) Colin, O., et al., "The 3-zones Extended Coherent Flame Model (ECFM3Z) for Computing Premixed/diffusion Combustion", *Oil & Gas Science and Technology Rev. IFP*, Vol. 59, No. 6 (2004), pp. 593-609.

Figs. 2-6 and 8-12

Reprinted from JSAE Paper, No. 20119137, Fuyuto, T., Matsumoto, T., Hattori, Y., Kugimoto, K., Fujikawa, T., Akihama, K. and Ito, H., "A New Generation of Optically Accessible Single-cylinder Engines for High-speed and High-load Combustion Analysis", © 2011 Society of Automotive Engineers of Japan, Inc.

Figs. 13-16

Reprinted from Proc. of COMODIA 2012, pp. 287-292, Fuyuto, T., Ueda, R., Hattori, Y., Akihama, K., Aoki, H., Umehara, T., Ito, H. and Kawaguchi, A., Analysis of CO Emission Sources in Diesel Combustion with Multiple Injections, © 2012 The Japan Society of Mechanical Engineers.

### Takayuki Fuyuto

Research Field:

- Engine Combustion

Academic Societies:

- The Japan Society of Mechanical Engineers

- Society of Automotive Engineers of Japan

- Combustion Society of Japan

Awards:

- Outstanding Technical Paper Award, Society of Automotive Engineers of Japan, 2009 and 2013

- Encouragement Award, Combustion Society of Japan, 2009

- Outstanding Presentation Award, Society of Automotive Engineers of Japan, 2011



---

**Yoshiaki Hattori**

Research Field:

- Engine Combustion

Award:

- Outstanding Technical Paper Award, Society of Automotive Engineers of Japan, 1997 and 2013




---

**Taketoshi Fujikawa**

Research Fields:

- Laser Diagnostics
- Visualization of Combustion
- Engine Combustion
- Intellectual Property

Academic Degree: Dr.Eng.

Academic Societies:

- Society of Automotive Engineers of Japan
- The Japan Society of Mechanical Engineers

Awards:

- Outstanding Technical Paper Award, Society of Automotive Engineers of Japan, 1992
- Research Award, The Japan Society of Mechanical Engineers Tokai Branch, 2007
- Outstanding Presentation Award, Society of Automotive Engineers of Japan, 2007




---

**Kazuhiro Akihama**

Research Fields:

- Laser Diagnostics/visualization of Combustion
- Combustion and Soot Formation Chemistry
- Engine Combustion

Academic Degree: Dr.Eng.

Academic Societies:

- Combustion Society of Japan
- Society of Automotive Engineers of Japan
- The Japan Society of Mechanical Engineers
- The Visualization Society of Japan

Awards:

- Encouragement Award, Combustion Society of Japan, 1998
- Outstanding Technical Paper Award, Society of Automotive Engineers of Japan, 2000, 2004 and 2013
- Research Award, The Japan Society of Mechanical Engineers Tokai Branch, 2007

